ICANS-VI

INTERNATIONAL COLLABORATION ON ADVANCED NEUTRON SOURCES

June 27 - July 2, 1982

DEVELOPING AN OPTIMUM TARGET DESIGN FOR A HIGH ENERGY SPALLATION NEUTRON SOURCE WITH RESPECT TO MECHANICAL AND THERMAL CONSTRAINTS

J.F.Stelzer

KFA Jülich

ABSTRACT

On the search for a suited target design different variants have been systematically been studied with respect to their temperature and rigidity behaviour. The calculations dealt with the temperatures and stresses in the maximally loaded parts and were carried out using the finite element method. The final solution is a rotating, internally water-cooled wheel of 2.5 m outer diameter, carrying about 9000 rods filled with lead. There are three highly loaded areas: the outer housing, the beam window and the lead-filled target rods. The construction of the mathematical models is shown. The results are introduced and discussed. The design satisfies the mechanical demands.

DEVELOPING AN OPTIMUM TARGET DESIGN FOR A HIGH ENERGY SPALLATION NEUTRON SOURCE WITH RESPECT TO MECHANICAL AND THERMAL CONSTRAINTS

J.F.Stelzer
KFA Jülich

1. THE SEARCH FOR A SUITED TARGET DESIGN

When our work on the target station started there existed two competing ideas how the problems arising with the extremly high heat deposition could be solved: 1) using a liquid metal circuit, and 2) using a rotating target wheel similarly like a rotating anode.

One of the most severe reasons speaking against the liquid metal circuit was the impossibility to find a acceptable window located between the pressurized liquid metal and the vacuum of the proton accelerating region. There is a certain thickness of the window necessary to withstand the fluid pressure, but the thicker the window the longer are the heat flux paths to the cooled surface and, consquently, the higher the temperatures and the thermal stresses. The appropriate relationships for a window consisting of graphite are exhibited in figure 1. Also windows of Molybdenum were examined as is reported in ref./1/ and /2/.

A concentration followed on Bauer's concept of a rotating target. The first proposal consisted in a compact lead target which was only cooled from its surfaces/3/. However, our finite element calculations of the temperature and stress distribution showed that the temperatures in the hottest region rose approximately to the melting temperature of lead, and the thermal stresses attained values beyond the tensile strength.

From this experience we learned that 1) the length of the heat flux paths from the region of the heat sources to the water-cooled surfaces need to be short, and 2) the lead volume should not be large and compact but distributed in several smaller sections to decrease the thermal stresses.

Consequently, a rotating target was proposed with evolvent-shaped lead sections with cooling water in the intermediate gaps, see ref./4/. A schematic picture of this design shows figure 2, and, addidionally, a scheme of the marching heat sources as considered in the calculations. However, an evaluation of the results showed that the maximal temperatures at the hot spots were still rather high, unless the evolvent width was small (<2 cm), and the thermal stresses could not yet be tolerated. The experience we gained from this was that the changing over from a compact 3-d-structure to a strip shape, a 2-d-structure, did not bring sufficient relief. The consequence was now to turn to a 1-d-configuration, where the target material is distributed in some thousand single rods which is the present concept. But before this design was studied for a certain time a compact target (also rotating) was examined where a partly melting of the lead was allowed.

Figure 3 gives an impression of the melting target concept. The beam enters with a flat angle and hits the inner surface. This design, however, cannot be realized because of the too high stresses in the housing. As material for the housing we proposed molybdenum or niobium since the intermediate temperatures in the hottest spot arise up to 1100 ^{o}C, but the thermal stresses increased to intolerable high values.

The described history of the Juelich target station shows the advantages resulting from a cowork between physicists who create always new proposals and ideas and engineers, in this case especially finite element analysts, who check in rather quick and not very expensive mathematical models the realisation possibilities. In this way by a chain of varied and stepwise improved designs an optimum can be found, or at least a compromise to live with.

As already mentioned, a provisionally final design exists. In this design some thousand single rods are fixed in a housing, as figure 4 displays. In the following the behaviour of this target wheel under thermal and mechanical loads is reported.

2. THE ANTICIPATED TARGET WHEEL DESIGN

A target wheel was chosen consisting of a slowly rotating, internally water-cooled wheel. With this concept it is possible to control the extremely high heat deposition (120 kW/cm^3 in a proton pulse peak) in such a way that neither the local temperatures nor the stresses exceed conventional limits, as will be shown. The calculations, throughout executed using the finite element analysis method, are concerned with those parts of the target which are subjected to the highest loads. These are

1) the rather weak housing which comprises the water-cooled, cylindrically-shaped target elements and which is mainly stressed by the water pressure,
2) that part of the housing which serves as the proton window and is exposed to intensive and intermittently acting thermal loads,
3) the target elements themselves which are stressed for a short time by a very intensive heat deposition resulting from the interaction between protons and matter. Some of these lead-filled cylinders have an additional task, working as tie-rods between the housing lid and the bottom and are thus additionally stressed.

The calculations were carried out using the FEABL2 programme. This programme was developed by A.Sievers, J.F.Stelzer and R.Welzel at the KFA Juelich, based on a software package developed by Orringer /6/. An advantage of this program is to calculate simultaneously temperature fields, structural deformations and stresses. Some routines had been adjusted to the special requirements of the task, as e.g. allowance for the pulsing character of the heat deposition by an accordingly fine incrementation of the time axis. The accompanying thermal stresses result for each time step from the momentary temperature distribution. Dynamic stress wave effects depending on a very rapid heating of the material as reported by P.Sievers /7/ were neglected in the calculations because this influence is very small under our operating conditions with pulse widths of 0.5 milliseconds.

Physical parameters. The heat sources in the exposed matter last for 0.5 milliseconds followed by a break of 10 milliseconds without heat deposition. The proton beam penetrates with a circular cross section. The corresponding heat sources form a Gaussian distribution across this area. The intensity decreases exponentially as it progresses through the target material. The relationships are shown schematically in Figure 5. Some data of the target wheel are given in table 1.

Table 1: Some target wheel data

outside diameter	250 cm
height of the target material (lead)	10 cm

depth of the area filled with target material in beam direction	70 cm
peripheral speed	4 m/s
speed of rotation	30.56 min^{-1}
angular velocity	3.2 s^{-1}

Our remarks concerning the three hard loaded design parts now begin with an examination of the stress behaviour of the target housing.

Rigidity analysis of the target housing. The outer casing of the water-cooled zone is made of AlMg3. It contains the lead filled, Al-clad target rods of approximately 24 mm outside diameter and 100 mm length, see figure 6. The casing houses about 9000 such rods. The casing bottom is thus stressed by the corresponding gravitational load. The main load, however, results from the coolant pressure. There are still other, but smaller loads resulting e.g. from the centrifugal forces acting in the water and the stagnation pressure at the outside wall. Because of its material and geometry the housing is not very rigid and its deformations become intolerable if all the rods are fixed according to figure 6.

The mathematical model. Figure 7 shows the calculation model. It is represented by 324 finite elements with 672 nodal points. Figure 8 gives some dimensions and the pressure distribution. In the actual structure the rods are located on 37 radii designated R1 to R37, from the largest radius to the smaller ones in the proton flight direction. The model has fewer opposite pairs of nodal points than rods. Therefore, with the connecting rods calculation a certain number of them is presumed to be combined at these locations.

Calculation results. Figure 9 shows the housing deformation if no special measures are undertaken. The maximum displacements of lid and bottom have approximately opposite positions and open a clearance of 2.13 mm. If target rods in this region are firmly connected to the opposite sheets, a considerable stiffening of the casing results. Figure 10 displays the deformation pattern with every second rod being fastened on the radii R16 and R18. In this way 272 rods act as traverses. The next two figures, 11 and 12, illustrate the reference stress distributions in the lid for both cases. The stresses remain tolerably low. The problem of the number and location of the traverses was the subject of an optimization procedure, see reference /8/.
The connecting rods altogether carry a total load of approximately 70 tons. The tensile stress in the rods will be superimposed by the thermal stress in a process described below. The same is true of the beam window which is also under tensile stress from the water pressure.

Rigidity analysis of the beam window. In addition to the mechanical load described, the beam window is also subjected to thermal stress by the proton beam. The protons arrive intermittently since the beam is pulsed. When the next proton flash enters the wheel has rotated further over a distance of one beam radius, see figure 13. This relationship establishs the context between the target wheel geometry and its rotating speed.

The mathematical model. This reproduces a part of the peripheral vertical sheet, see figure 14. The curvature is not taken into consideration with regard to the rather large radius. The following data are used, table 2.

Table 2 Data of the beam window

Material	Al Mg3
sheet thickness	5 mm

proton beam radius 40 mm
maximum heat deposition 47 kW/cm^3
water cooling from the rear with 1 W/(cm^{2}K)
water temperature 30 ^{o}C.

Cooling is only effected from the rear since the front is surrounded by vacuum. For the calculation it is assumed that an appropriate angular range of the window stays in the beam for 0.5 milliseconds. After 10 milliseconds the next spot is hit, the centre of which is one radius distant from the former one. The same cross section is once again immersed in the heat deposition area after 2 seconds. Cooling is continuously maintained. For reasons of symmetry only the hatched half of the window needs to be taken into consideration. The transient temperature field calculation takes the moving heat sources into consideration in the manner mentioned. The initial temperature is 30 ^{o}C.The results from the casing calculation must also be introduced. This is performed by including the found radial and axial displacements as constraints in the window calculation, as is shown diagrammatically in figure 15.

Results. The calculation reveals that the quasi steady-state relationships are attained after 6 target wheel revolutions. The temperature distribution occuring immediately before heat deposition is illustrated in figure 15. The proton shot then causes the temperatures which are given in figure 16. The maximum temperature rise amounts to about 11 K. The stresses (here: the reference stresses) in the element centres can be seen in figure 18. An evaluation of the stresses is made at the end of the paper.

Temperatures and stresses in the target elements. A target rod has a cylindrical shape, is filled with lead and clad with AlMg3. Similarly to the beam window, every rod stays for a short time in the proton beam before it is carried away by the rotating wheel. Thus, from shot to shot hitting the same spot a rather long cooling period occurs.

The calculations deal with target rods in different positions. The highest thermal load is induced in the rods on the largest radius (R1). The calculations also take the rods on the radii R16 and R18 into consideration. There is only a reduced thermal stress here since the incoming proton energy is already weakened by the 30 cm path through an energy absorbing zone. On the other hand, these rods must bear the tensile load due to their function as through-bolts discussed above. Some variants with different cladding thicknesses were calculated since the cladding must take over the main part of the tensile load because of the weakness of the lead.

The mathematical model. This is shown in figure 19. For reasons of symmetry only one quarter needs to be simulated. The subdivision into finite elements is accomplished in three storeys. The limiting planes between them where the nodal points are situated are designated Z0 to Z3. Each storey is subdivided into 126 finite elements as can be seen in figure 20. On the outer surface of the model a heat transfer coefficient of 1 W/(cm^{2}K) is assumed. At the beginning of the transient temperature field calculation the whole rod is at the temperature of the cooling water. During the calculation a constant ambient fluid temperature is assumed.

Heat deposition. The pulsing heat deposition is again observed with 5 ms heating followed by 2 s cooling time. The Gaussian distribution of the heat deposition over the beam radius and the exponential axial decrease are taken into account. However, the heat source decrease across one rod does not

amount to more than 10 %.

Pre-stressing. The case was also considered in which the lead kernel is undercooled before being inserted into the AlMg3 cladding to prevent a gap between the kernel and the cover. The tangential initial stress of 50 N/mm^2 is appropriate. But there is little danger that such a gap and an associated temperature rise will occur since the lead shows a larger thermal expansion (about 20 %) than the AlMg3. An axial pre-stress appears in the rods acting as traverses. This load is induced by constrained displacements resulting from the casing analysis.

Results. Temperatures. Let us first consider a rod on the largest radius. The time dependent temperature development is exhibited in figure 21 for the hottest point of a rod. After about 10 s or 5 wheel revolutions a stable state is reached. The rise between the temperature extremes amounts to 42 K. A survey of all nodal point temperatures is given in figure 22. The temperature exceeding that of the cooling water in the centre of the rod middle plane (Z3) varies between 21 and 63 K. The outer AlMg3 jacket is 15 K above the coolant temperature. The leaving heat flux density amounts to 15 W/cm^2. This means a very large interval between subcooled boiling (which is not dangerous at all), not to speak of the dangerous film boiling which would not appear before 300 W/cm^2. Despite the rather low melting point of lead (327 ^oC) no melting will take place. With a coolant temperature of for example 60 ^oC the highest lead temperature will be at 123 ^oC.

Stresses are calculated in the geometrical centres of the finite elements. In the non-prestressed rods the stresses are only a consequence of the temperature gradients and the impeded thermal expansion of the lead restrained by the influence of the AlMg3. Tangential and axial stress components predominate. Figure 23 illustrates the reference stress distribution in the layer with the highest load which is located between the planes Z2 and Z3. The maximum reference stress appears in the AlMg3 jacket and amounts to 75 N/mm^2. In the case of pre-stressing by shrinking, the maximum stress rises to 109 N/mm^2.

A hypothetical operating disturbance. Some problems could perhaps arise if the coolant flow were partly blocked e.g. by distorted or disconnected target rods. It may be assumed that then the heat transfer along half of the target rod surface decreases to one tenth, to 0.1 $W/(cm^2K)$. In the central plane of the rod temperatures then occur as shown in figure 24. The highest overtemperatures above the coolant now vary between 72 and 112 K. It can be seen that even such a severe deterioration of local cooling does not provoke a dangerous temperature increase.

Temperatures and stresses in the through-bolt rods. These rods are located in the radii R16 and R18. The proton beam only deposits about one quarter of the heat sources here compared to the radius R1. The maximum temperature variations range between 5 and 15 K above the coolant temperature. The stresses were calculated for jacket thicknesses of 0.5 and 1 mm and thermal and tensile load. The tangential pre-stress caused by a shrunken jacket was also taken into account. The results are listed in the following table 3.

Table 3: Maximum stresses in the cladding of a rod on R18, layer between the planes Z2 and Z3, in N/mm^2

Cladding thickness (mm)	tangential pre-stress	tensile load	σ_r	σ_ϕ	σ_z	σ_{ref}
0.5	no	no	0.04	12.4	12.8	12.7

0.5	yes	no	-0.9	57	15.2	51.8
0.5	yes	yes	-0.9	57.3	21.6	50.9
1	no	no				11
1	yes	no				47
1	yes	yes				47

It can be seen that the stress reduction by a doubling of the cladding thickness is insignificant. A tangential pre-stress is responsible for a high stress increase. The maximum reference stress in the lead is 5.9 N/mm^2.

3. FINAL EVALUATION OF THE RESULTS

As has been shown, in the design the temperatures remain at low and non-critical values at all locations. In order to evaluate the stresses we must refer to the appropriate tolerable stresses. Because of continuous cyclic loading the fatigue stress should preferably be taken into consideration. AlMg3 in a soft, annealed state is in this respect superior to hard, cold-formed material. The following values are given in ref. /9/, table 4.

Table 4: Fatigue strength of AlMg3 in N/mm^2 under cyclic loading with alternating tensile and compressive stress

state	lower limit	upper limit
soft	72	126
semihard	58	115
hard	52	78

At two locations on the target the lower limit of the soft material is slightly exceeded: in the centre of the beam window (stress equals 75 N/mm^2) and in the rod jacket of a rod on the outer radius (also 75 N/mm^2). We see that it is not advisable to shrink the jackets on the rods since then the stress will increase to the intolerable value of 109 N/mm^2.

It can thus be seen from the results that an arbitrarily long lifetime of the target assembly cannot be expected. This would undoubtedly be the case if the maximum stress were to remain everywhere below the lower fatigue strength limit. However, from the engineer's point of view it can be stated that the thermal and mechanical loads occuring in the target wheel do not exceed tolerable and commonly accepted limits.

References

/1/ SNQ Realisationsstudie zur Spallations-Neutronenquelle, ed.G.S. Bauer, H.Sebening, J.Vetter, H.Willax, Jül-Spez-113, Jülich, 1981, 3 volumes

/2/ Seitz, L., A.Sievers, J.F.Stelzer: Strahlfenster unter thermischer und mechanischer Belastung, chapter 42 in vol.3 of /1/

/3/ Stelzer, J.F.: Heat dissipation and thermal stress in solid targets, paper at the Meeting on Targets for Neutron Beam Spallation sources, Juelich, 11-12 June 1979

/4/ Emmerich, R., L.Seitz, J.F.Stelzer: Temperatures and thermal stresses in a spallation target from lead, evolvent target, chapter 41 in vol.3 of /1/

/5/ Seitz, L., A.Sievers, J.F.Stelzer: A rotating target from lead with phase change solid-liquid, chapter 40 in vol.3 of /1/

/6/ Orringer, O., S.E.French: FEABL finite element analysis basis library, AFOSR TR, ASRLTR 162-2, MIT, Cambridge, Mass., 1972

/7/ Sievers, P.: Elastic stress waves in matter due to rapid heating by an intense high-energy particle beam, European Organization for Nuclear Research, paper LAB II/BT/74-2, Geneva, 1974

/8/ Stelzer, J.F.: Two applications of optimum structural design in the field of nuclear technique, Proc. Int.Symp. on Optimum Structural Design, ed. R.H.Gallagher, E.Atrek, A.J.Morris e.a., University of Arizona, Tucson, 1981, pp.1-23 to 1-29

/9/ Sass,F. and Ch.Bouchê, editors: Dubbels Taschenbuch für den Maschinenbau, 11th ed., Springer, Berlin, 1958, pp.540-542

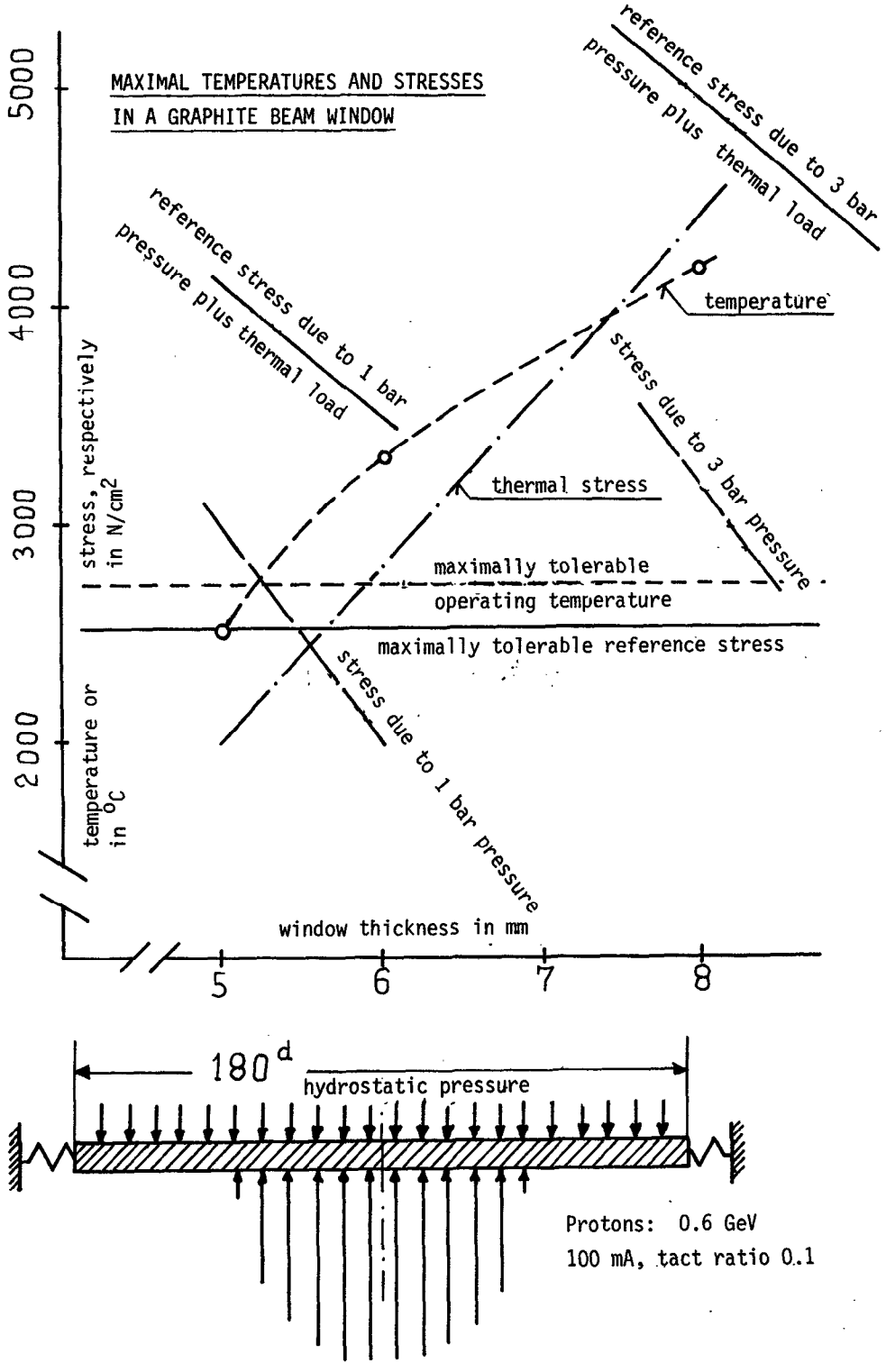

Fig. 1. Maximum temperatures and stresses vs. window thickness in a beam window of graphite. Heat deposition according to the anticipated Juelich spallation source.

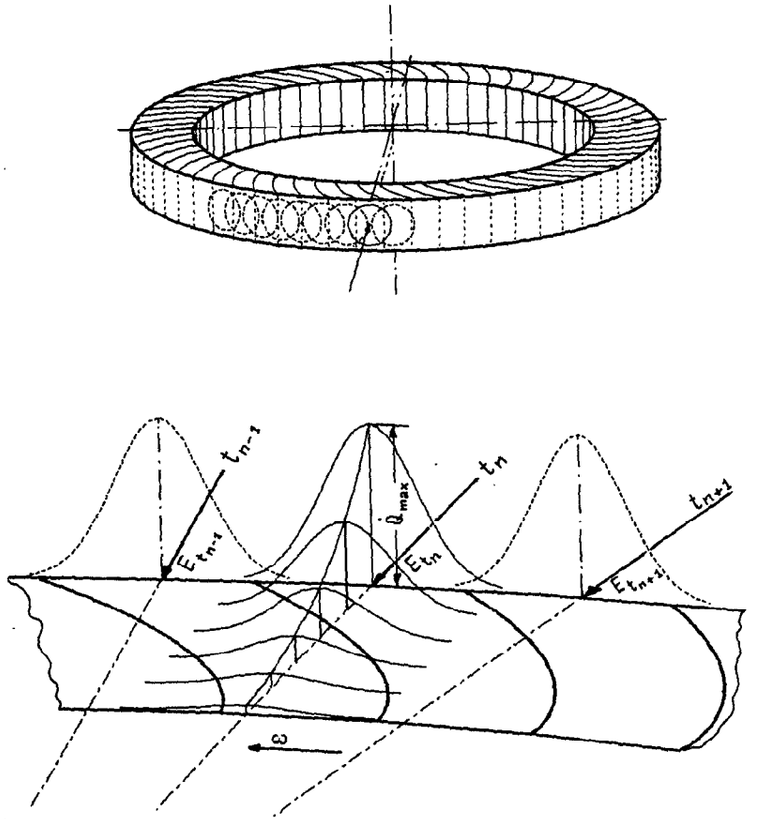

Fig. 2. Scheme of the evolvent-shaped target wheel (above) and of the marching heat sources (below)

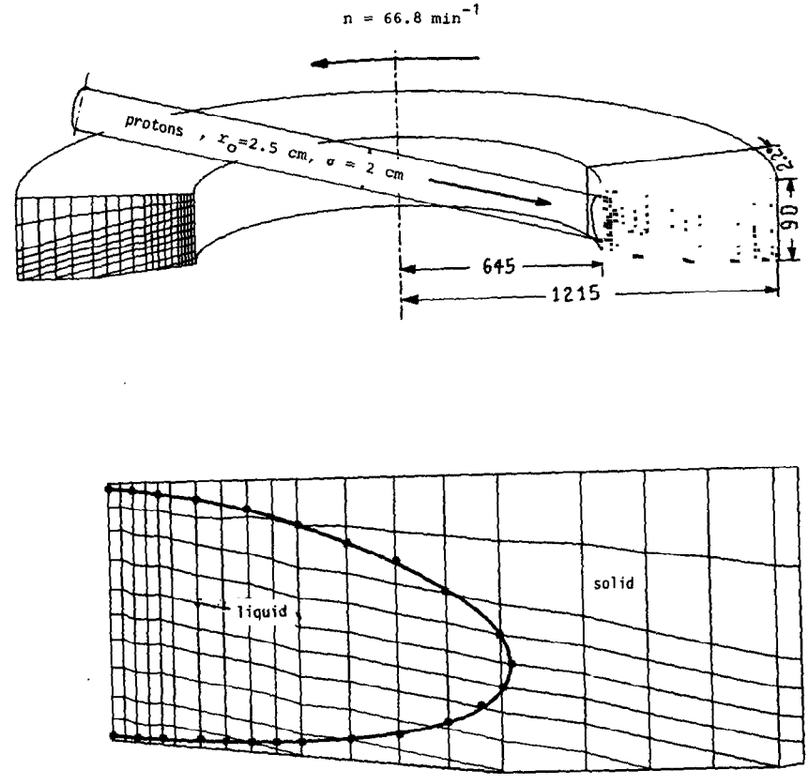

Fig. 3. Melting target with the finite element subdivision (above). Calculated areas of molten and solid lead after 80 target wheel revolutions, quasi-steady-state (below).

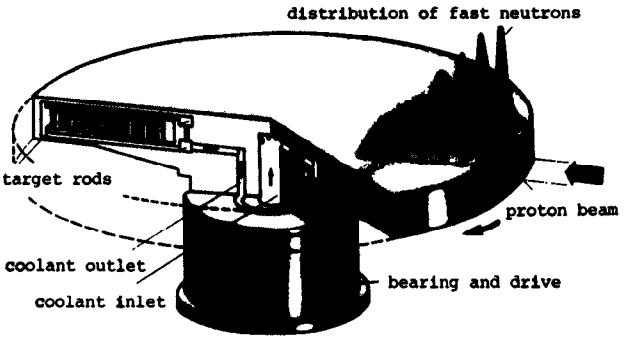

Fig. 4. Survey of the target wheel which suits all thermal and mechanical demands

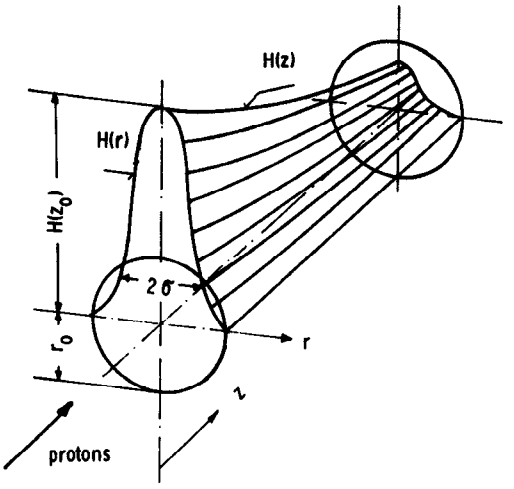

Fig. 5. Distribution of the induced heat deposition in a solid body by proton bombardment

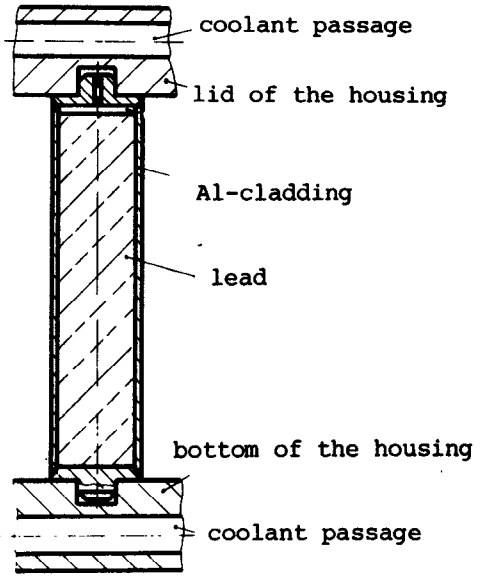

Fig. 6. A single target rod. It is situated in the wheel housing with plugs at both ends. It can expand independently of the ambient rods.

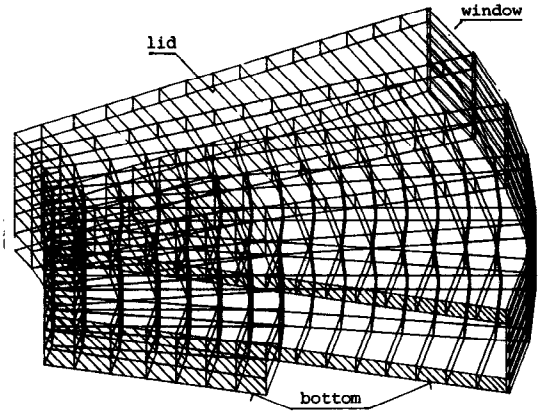

Fig. 7. Projected view of the calculation model

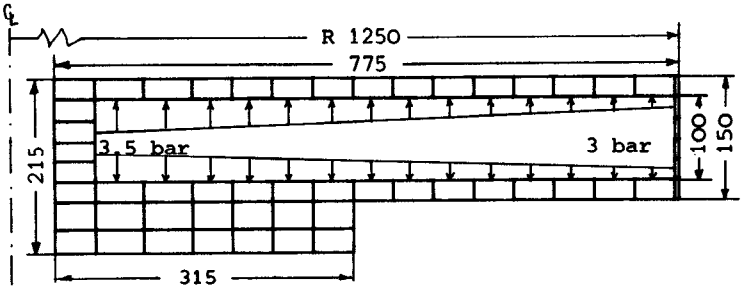

Fig. 8. A model cross section

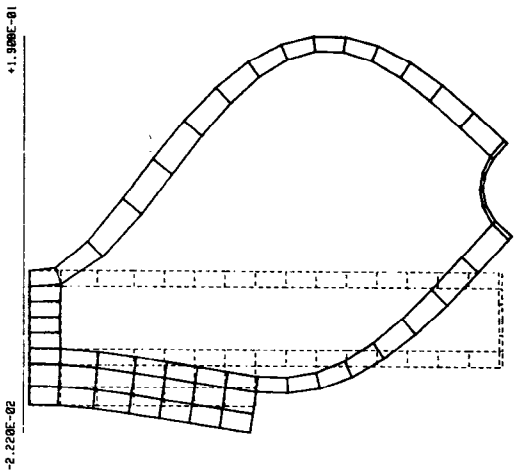

Fig. 9. Deformation of the housing if no traverses are present. Deformation enhancement by a factor of 200.

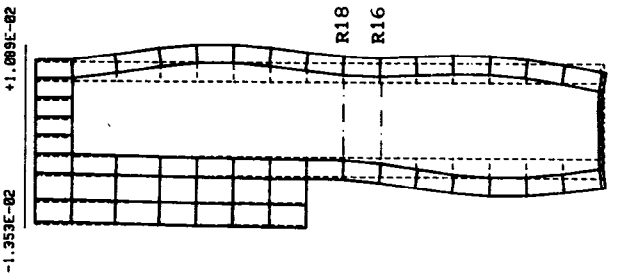

Fig. 10. Deformation of the housing with traverses at the radii R16 and R18. Deformation enhancement by a factor of 200.

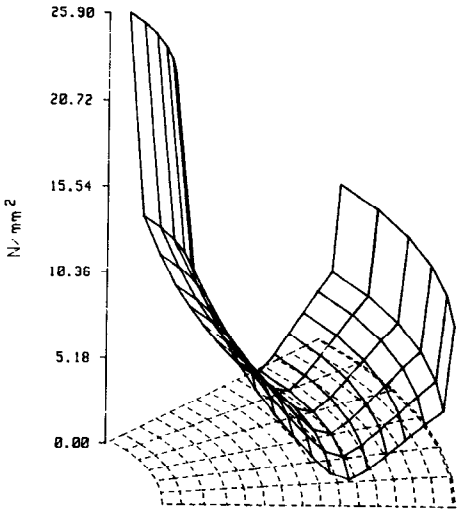

Fig. 11. Distribution of the reference stresses in the lid of the housing if no traverses are present

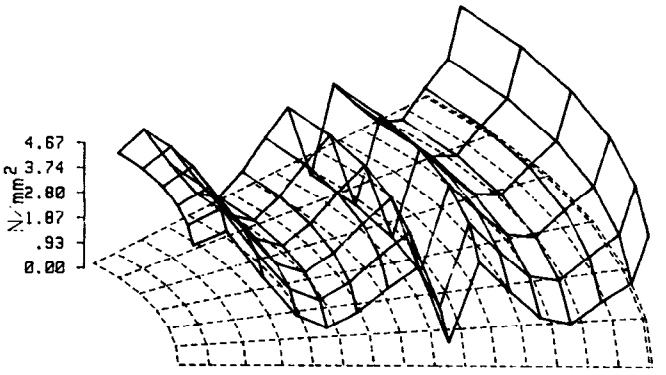

Fig. 12. Reference stress distribution in the lid of the housing with traverses in the radii R16 and R18

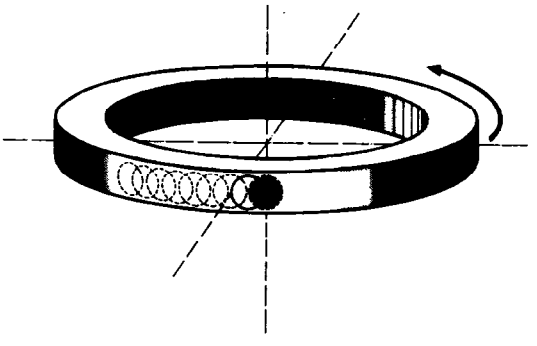

Fig. 13

The chronological order of energy deposition in the outer wheel wall, the window

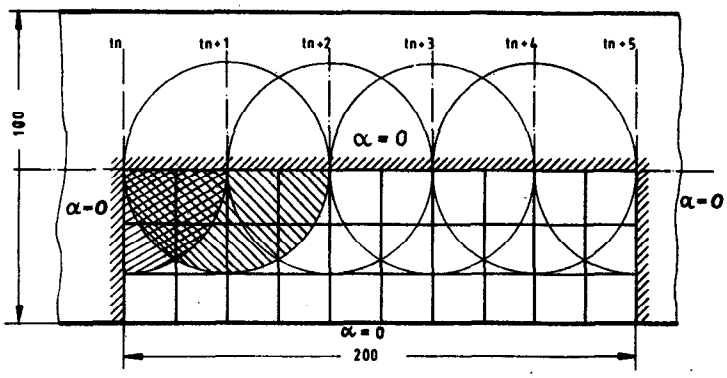

Fig. 14

Mathematical model of the beam window

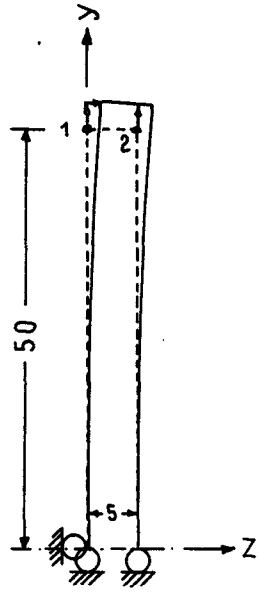

Fig. 15

Displacement constraints of a window cross section

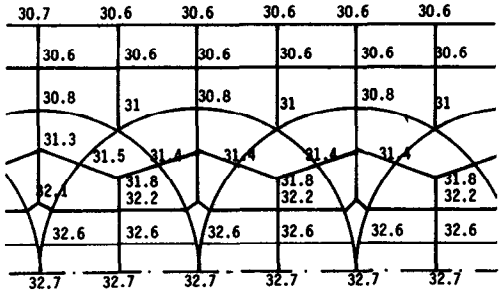

Fig. 16. Temperature distribution in the window after 2 s cooling shortly before heat deposition, quasi-steady-state, in centigrade

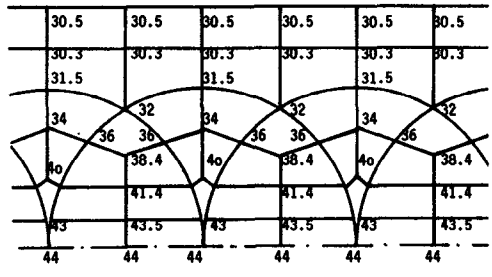

Fig. 17. Temperature distribution in centigrade in the window immediately after heat deposition

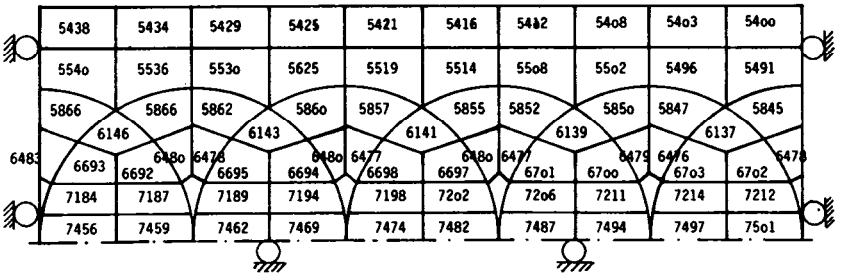

Fig. 18. Reference stresses in the beam window in N/cm^2

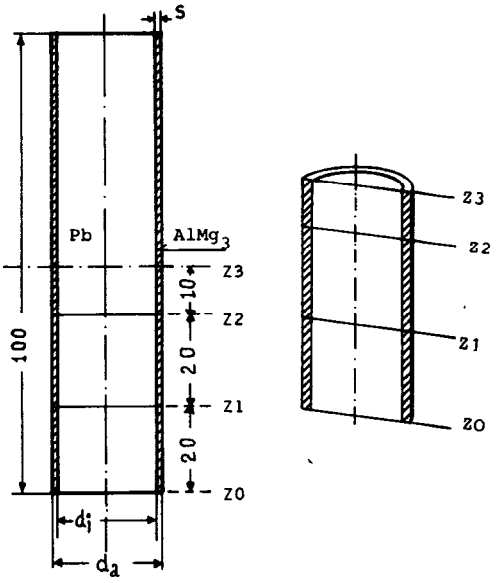

Fig. 19

Mathematical model of the target rod. It consists of three finite element storeys. The intermediate planes are designated Z0, Z1, Z2 and Z3.

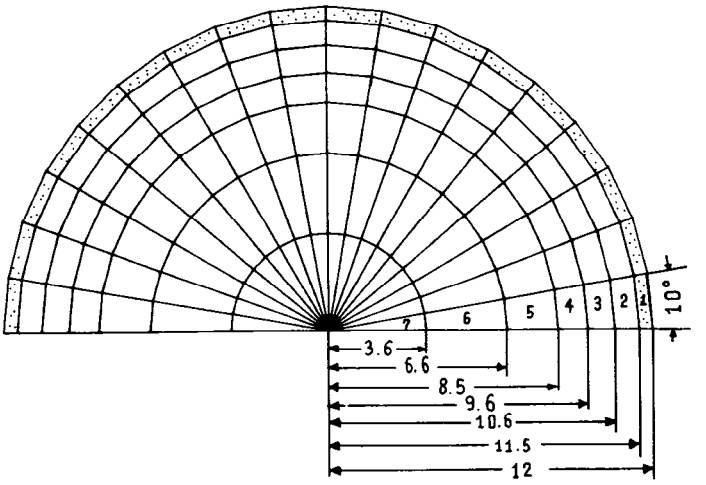

Fig. 20

Plane with nodal point

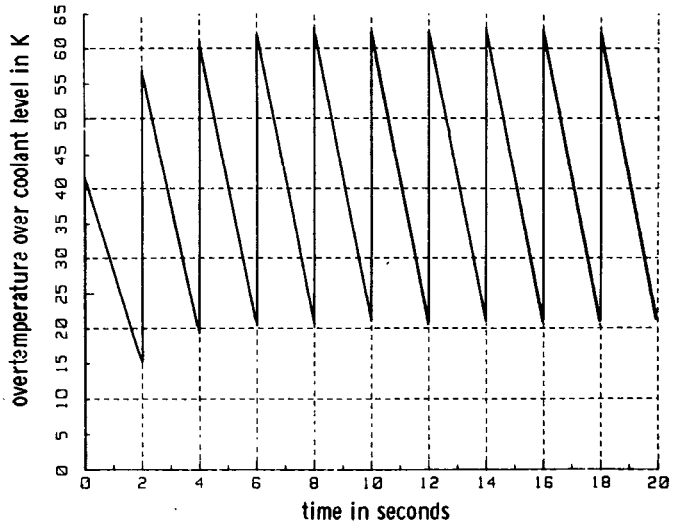

Fig. 21

Time-dependent development of the temperature at the hottest spot of a target rod on the largest radius

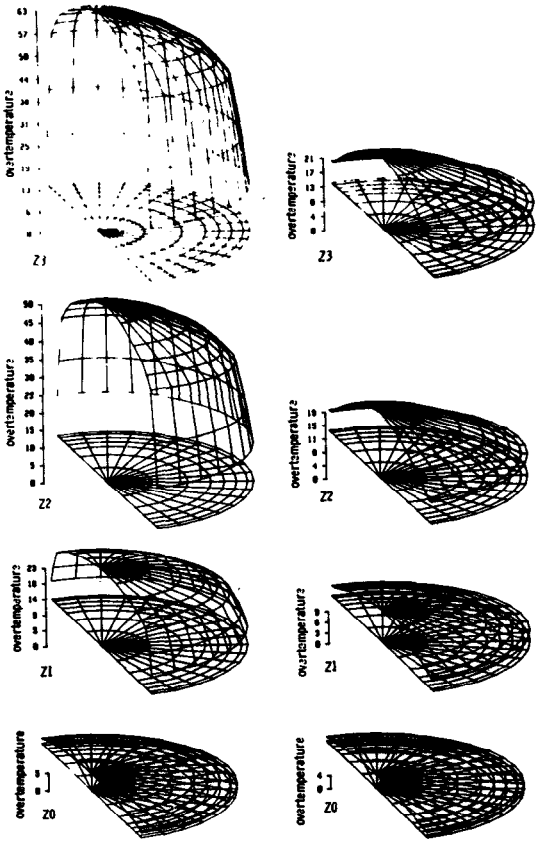

Fig. 22

Temperatures in the four planes of the target rod. Left column: immediately after energy deposition, right column: after an intermediate cooling time of 2 s.

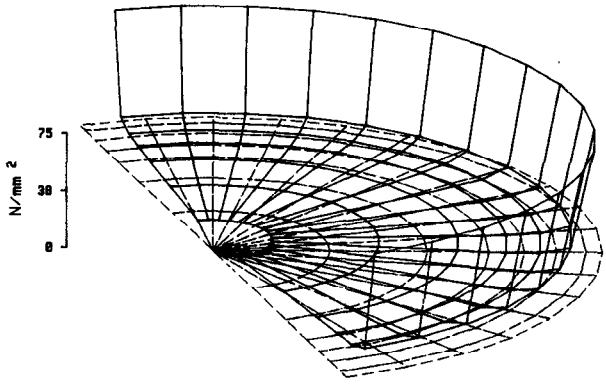

Fig. 23

Distribution of the reference stresses in the target rod in the region of the highest load

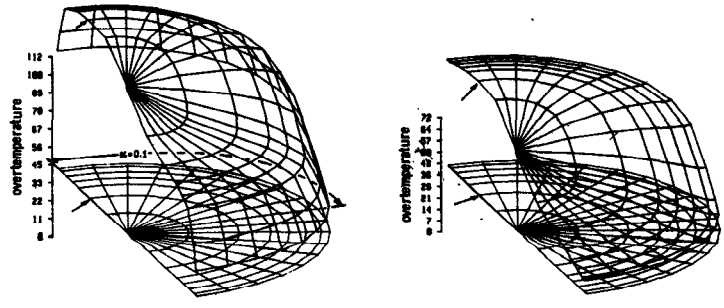

Fig. 24

Temperatures in a target rod, plane with the maximum temperatures in the context of a coolant flow disturbance. Left: after the shot, right: after 2 s cooling.